ACS APPLIED MATERIALS & INTERFACES

Surfaces, Interfaces, and Applications

P-n Sensitized Heterostructure Co3O4/Fullerene with Highly Efficient Photoelectrochemical Performance for Ultrasensitive DNA Detection

Hai-Hua Wang, Meng-Jie Li, Hai-Jun Wang, Yaqin Chai, and Ruo Yuan

ACS Appl. Mater. Interfaces, **Just Accepted Manuscript** • DOI: 10.1021/acsami.9b05923 • Publication Date (Web): 06 Jun 2019

Just Accepted

is published by the American Chemical Society. 1155 Sixteenth Street N.W., Washington, DC 20036

P-n Sensitized Heterostructure Co_3O_4/Fullerene with Highly Efficient Photoelectrochemical Performance for Ultrasensitive DNA Detection

Hai-Hua Wang, Meng-Jie Li, Hai-Jun Wang, Ya-Qin Chai*, Ruo Yuan*

Key Laboratory of Luminescence and Real-Time Analytical Chemistry (Southwest University), Ministry of Education, College of Chemistry and Chemical Engineering, Southwest University, Chongqing 400715, People's Republic of China

Abstract

Significantly sensitized architectures meeting the requirements of high photoelectric conversion efficiency and promising photocurrent intensity are extremely desirable but remain challenges on sensitizer development and sensitized efficiency in PEC fields. In this paper, p-type metal oxide semiconductor Co_3O_4 was attached as effective photosensitizer to n-type fullerene C_{60} in view of appropriately-matched energy band levels to form the highlighted p-n sensitized heterostructure Co_3O_4/fullerene, with facilitated charge separation and accelerated carrier mobility. Compared with traditional p-n heterostructure, the p-n sensitized heterostructure Co_3O_4/fullerene illustrated wider range for light absorption with further enhanced light-harvesting capability, thereby leading to more exceptional PEC performance containing remarkably promoted photoelectric conversion efficiency and improved

* Corresponding author. Tel.: +86-23-68252277; Fax.: +86-23-68253172.

E-mail address: yqchai@swu.edu.cn, (Y. Q. Chai), yuanruo@swu.edu.cn (R. Yuan)

photocurrent intensity. Impressively, the photocurrent intensity obtained by Co_3O_4/fullerene was about 6-fold higher than that of fullerene alone, and this achievement was quite favored compared to the reported works for fullerene sensitization, which could be responsible for the advancement of detection sensitivity for the subsequently constructed biosensor. Unambiguously, given the p-n sensitized heterostructure Co_3O_4/fullerene of high PEC activity, the well-fabricated three-dimensional DNA Walker applied as target-cascade signal amplification strategy, and Au layer employed as the specific linker between the photoactive material and the signal amplification product, a smart photoelectrochemical (PEC) biosensor was successfully enabled for ultrasensitive investigation of the model DNA (a fragment of p53 gene), showing a wide linear range from 60 aM to 1×10^5 aM and a detection limit of 20 aM. This proposed PEC biosensor provided acceptable insights to the clinic analysis, disease therapies and other relevant subjects.

Keywords: Photoelectrochemical; p-n sensitized heterostructure; fullerene; Co_3O_4; signal amplification

Introduction

Photoelectrochemical (PEC) technique has attracted substantial research due to the instinct advantages of accessible operation, rapid response and ultrahigh sensitivity.[1, 2] Fundamentally, sophisticated photoactive materials are responsible for the fabrication of exquisite PEC schemes.[3, 4] Over the past few years, quantum dots (QDs) that can be prepared accessibly and easy to modify for efficacious biocompatibility are typically developed in PEC platforms.[5, 6] Very recently, Tang's group applied the 'Z-Scheme' nanohybrids[2, 7] and upconversion nanomaterials[8, 9] of intrinsic characteristics in PEC detection systems, coupling

with next-step significant applications. Inspired by these emerging exploration, notably, sensitization structures, with sensitizers typically attached to the basic photoactive materials, are playing an increasingly vital role in obtaining distinctive PEC manifestation.[10, 11] By giving prize to the range broaden of light-harvesting and facilitation of electron-hole separation, smart fabricated sensitizations have been proved to enjoy greatly enhanced photoelectric performance to obtain increased photocurrent intensity. Up to now, two main types of sensitizers, QDs[12, 13] and organic dyes[14, 15], are collectively employed in the typical sensitization structures, and light achievements have been acquired. However, it is well-known that QDs inevitably endure variable quantum yield and biological toxicity.[16] Besides, previous reporter have proved an inherently fragile optical stability marked as static and dynamic disorder for organic dyes.[17]. These disadvantages greatly hinder further applications of QDs and organic dyes in PEC fields. To this end, it is expected to hunt for more desirable photoactive sensitizer to form novel exceptionally sensitization structure in PEC architectures.

As abundant, available synthesis process and non-toxicity substrates, transition metal oxide semiconductors are strikingly unique and free from the shortages of quantum dots and organic dyes.[18] Among them, p-type cobalt oxide (Co_3O_4) that owns two noticeable direct transitions with strong absorption in the visible light range, exhibits appropriate optical band gap with vivid electron-hole separation, and possesses stable PEC behavior over a broad range of pH values, have attracted especial investigation and been widely used.[19, 20] Benefiting from the outperformed PEC activity of Co_3O_4, noticeable breakthroughs have focused on the Co_3O_4-comprised p-n heterostructures, such as p-n heterojunction $Co_3O_4/BiVO_4$ photoanodes highlighted by enhanced surface reaction kinetics and charge separation.[21] Despite the effort,

behind such a conventional p-n heterostructure, poorly increased ability of light absorption was acquired, of which the wide range harvest of visible light from approximately 500 nm to 800 nm was found to be still restricted although the accomplishment of the p-n heterostructure. In addition, its further improvements of the photoelectric activity suffer from the inherent disadvantage of the destitute electronic affinity. These suggest amelioration requirements of photoelectric performance towards the conventional p-n heterostructure.[22]

Notably, it is gratifying that p-n sensitized heterostructures could overcome the shortages mentioned above to meet the requirements of more distinctive PEC manifestation, *via* emphasis of the strong donor-acceptor interaction and improvement ability of light capture not only to enlarge of light absorption range, based on the well-matched optical band gap and energy level.[23] As classic carbon nanomaterial, n-type fullerene C_{60} of delocalized conjugated structure exhibits strong electron-accepting ability and exceptional photoinduced charge mobility.[24, 25] In view of the merits of fullerene, a novel p-n sensitized heterostructure Co_3O_4/fullerene was fabricated in this work, which implemented markedly promoted visible light absorption, facilitated electron-hole separation, and accelerated charge carrier mobility. Compared with the conventional p-n heterostructure $Co_3O_4/BiVO_4$, wider range for light absorption expanding to the whole solar spectrum, further promoted photoelectric conversion efficiency and enhanced photocurrent intensity of the p-n sensitized heterostructure Co_3O_4/fullerene were illustrated as expected, making the latter more appropriate candidate in catalyst activity, water oxidation, and biosensing.

Herein, a smart PEC biosensor was successfully proposed for ultrasensitive detection of the model DNA (a fragment of p53 gene) based on the p-n sensitized heterostructure

Co_3O_4/fullerene and the cascade signal amplification strategy, as illustrated in Scheme 1. At first, the basic n-type photoactive nanomaterial fullerene and its p-type sensitizer Co_3O_4 were successively anchored on the electrode to form the p-n sensitized heterostructure Co_3O_4/fullerene, leading to high and stable photocurrent intensity. While the prepared DNA Walker-protection DNA (DW-PD) and signal DNA-SiO_2 (SD-SiO_2) bioconjugates were later incubated on the surface of modified electrode, an intense decrement of the photocurrent response was acquired for the dramatic appearance of steric hindrance from SiO_2 NPs.[26, 27] Subsequently, the introduction of output DNA traced from the Nt.BstNBI enzyme-assisted target recycling amplification (Cycle Ⅰ) could trigger the 3-D DNA Walker recycle amplification (Cycle Ⅱ) on electrode surface. Concretely, output DNA was competitively hybridize with the protection DNA, making the DW release from the DW-PD *via* a toehold exchange mechanism, and then the DW would move and specifically hybridize with SD-SiO_2. Under the designated recognition and cleavage effect of the Nb.BbvCI enzyme, the SD-SiO_2 segment could be digested rapidly to effectively detach the signal quencher SiO_2, leading to adequate recovery of the photocurrent intensity, which was employed to quantitatively determine the target DNA (a fragment of p53 gene). Collectively, a wide linear range from 60 aM to 1×10^5 aM and a detection limit of 20 aM were obtained. As a proof-of-concept application, this PEC platform opened a fascinating avenue in the construction of desirably sensitized photoactive candidates with predominant PEC performance, and exhibited significant application foreground in the determination of biomolecules.

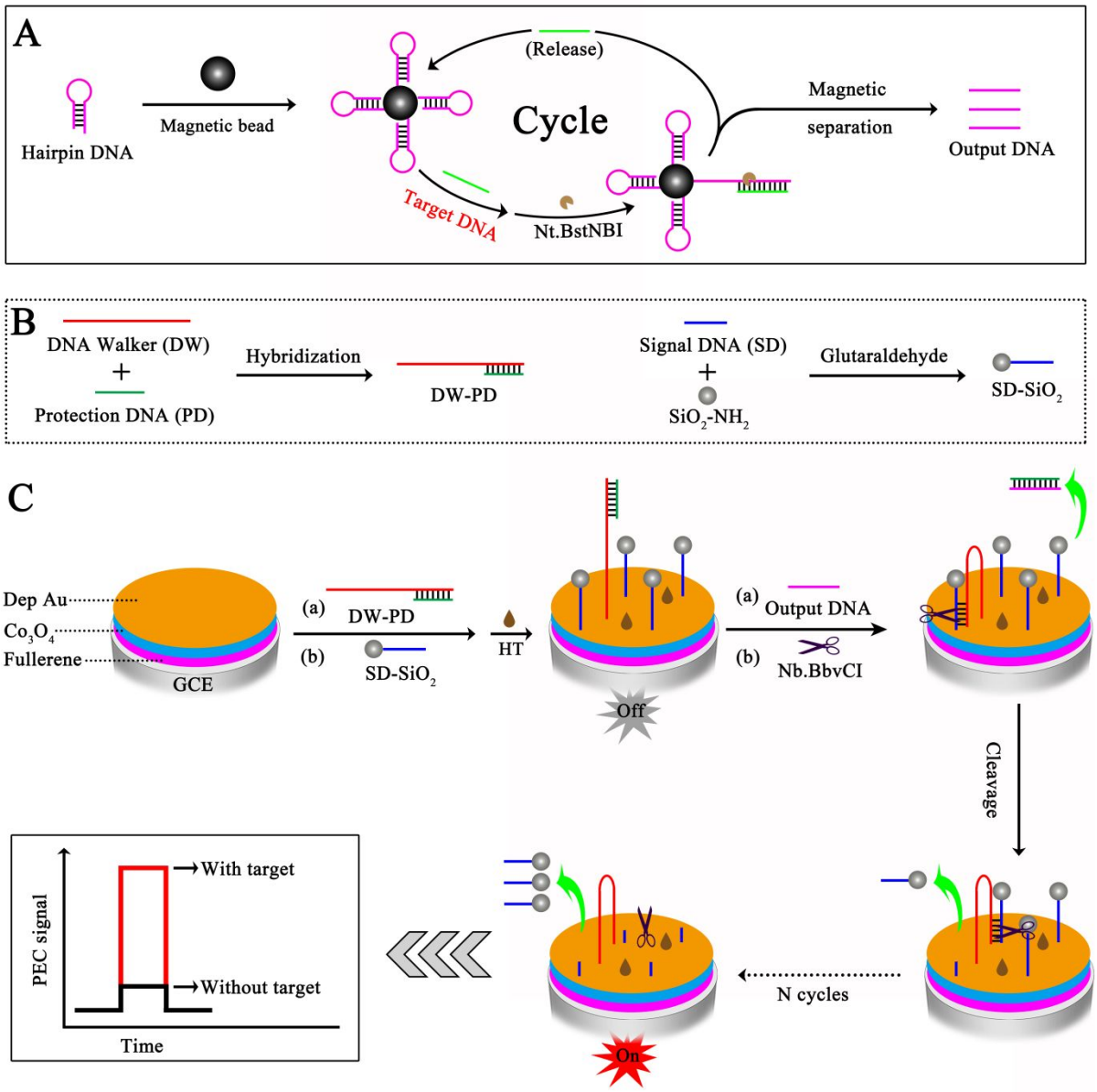

Scheme 1. Schematic illustration of (A) the enzyme-assisted target recycling amplification; (B) the synthesis of DW-PD and SD-SiO_2; (C) the fabrication procedure of the PEC biosensor with the PEC responses in the absence/presence of target.

Experimental Section

Synthesis of Fullerene and Co_3O_4 Dispersions.

Firstly, 2 mg fullerene particles was added to 2 mL toluene with violent shake to obtain a fuchsia homogeneous solution. Then 2 mL deionized water was introduced to the above

solution and the resulted mixture was treated ultrasonically for about 24 h to thoroughly get rid of the toluene. Ultimately, the obtained buff fullerene dispersion was kept for further use.

Co_3O_4 was prepared *via* the facile hydrothermal method based on the previous literature with some modifications.[21] In a typical procedure, 2 mL $NH_3 \cdot H_2O$ was added to 50 mL 2 mM $Co(CH_3COO)_2$ aqueous solution with rapid stir for 1 h to get a homogeneous phase, then the mixture was delivered to a 100 mL Teflon-lined stainless steel autoclave that was followed to be conducted at 150 ºC for 3 h. Next, the autoclave was cooled naturally and the obtained product was centrifugally treated with deionized water for three times. Finally, the precipitation was dried at 100 ºC for 5 h and the harvested Co_3O_4 samples were dispersed in 5 mL ethanol to get Co_3O_4 dispersion for further use.

Nt.BstNBI Enzyme-Assisted Target Recycling Amplification.

At the beginning, 20 μL Fe_3O_4@Au NPs suspension was added to 100 μL hairpin DNA with gently stir at 4 ºC for 16 h to make the hairpin DNA covalently connect with MB through Au-S bonds, followed by introducing with 60 μL target DNA and incubating at 37 ºC for 0.5 h to conduct the hybridization between target DNA and hairpin DNA. Subsequently, the above mixture was treated with 10 μL Nt.BstNBI enzyme (10 U) and 15 μL 10 × NE Buffer at 55 ºC for 1 h to accomplish the enzyme-assisted target DNA recycling amplification, and then heated to 80 ºC for 20 min to deactivate the Nt.BstNBI enzyme. Lastly, after the solution was cooled down to room temperature naturally, the output DNA was collected magnetically.

Fabrication of the PEC Biosensor and the Nb.BbvCI Enzyme-Assisted 3-D DNA Walker Amplification.

Before building the biosensor, the mixture of 50 μL DW and 50 μL protection DNA was

incubated at 37 ºC for 2 h to obtain DW-PD double-strands. 100 μL SiO_2-NH_2, 20 μL amino-terminated signal DNA, and 5 μL glutaraldehyde were mingled under stirring for 1 h to get the SD-SiO_2 bioconjugates. In addition, pretreatment for the bare glass carbon electrode (GCE) was similar to our reported work.[14]

To fabricate the PEC biosensor, at first, 5 μL fullerene dispersion and 10 μL Co_3O_4 dispersion was coated onto the pretreated electrode to gain flimsy layers. Then an Au film on the modified electrode surface was obtained with the electrode electrodeposited in 1% $HAuCl_4$ solution at -0.2 V for 15 s (dep Au), where Au was treated as a marvelous immobilization element for the next-step DNA attachment benefiting from its great aqueous stability and bimolecular affinity. Afterwards, 15 μL DW-PD and 15 μL SD-SiO_2 were consecutively attached to the electrode surface through Au-S bonds at 4 ºC for 16 h, followed by anchoring with 15 μL hexanethiol (HT) (1 mM) for 40 min to hinder the nonspecific binding sites. As 15 μL output DNA was subsequently incubated, the protection DNA competitively hybridized with the output DNA, making the DW release to further hybridize with the SiO_2-labeled signal DNA. Later, when 3 μL Nb.BbvCI (10 U) enzyme and 15 μL 10 × NE Buffer was incubated, the signal DNA of SD-SiO_2 bioconjugates could be specifically cleaved, so the element SiO_2 was rapidly departed and the DW was simultaneously released to trigger the next cleavage. Lastly, the obtained electrode was incubated at 80 ºC for 20 min to inactivate the Nb.BbvCI enzyme. The electrode was completely cleared after each step to get rid of the physically absorbed substrates.

Results and Discussion

Characterizations of the Synthesized Nanomaterials.

Transmission electron microscopy (TEM) and high-resolution transmission electron microscopy (HRTEM) were applied to characterize the morphology for the synthesized nanomaterials. Figure 1 illustrated that the monodisperse fullerene and Co_3O_4 both exhibited uniform globular structure, with an average diameter of ca. 30 nm for fullerene (Figure 1A and 1B) and ca. 4 nm for Co_3O_4 (Figure 1C and 1D), respectively.

In the model for chemical impedance spectroscopy (EIS) measurements, a smaller semicircle diameter indicated a superior ability for electron transmission. As can be seen from Figure 2B, the fullerene/GCE showed a big semicircle diameter (curve a), while a small semicircle diameter was found towards the Co_3O_4/fullerene/GCE (curve b), revealing the enhanced charge separation and accessibly improved capability for electron transmission of the p-n sensitized heterostructure Co_3O_4/fullerene. Besides, compared with the light-harvested capability of pure fullerene (curve a), that of Co_3O_4/fullerene (curve b) was enhanced remarkably in entire visible range and part ultraviolet region through the ultraviolet-visible (UV-vis) absorption spectrum absorption spectrum in Figure 2C, suggesting an improvement of subsequently PEC activity of the p-n sensitized heterostructure Co_3O_4/fullerene. Studies for the correspondent photocurrent intensity of the different photoactive nanomaterials showed that ca. 0.95 μA (Figure 2D, curve a) and ca. 0.85 μA (Figure 2D, curve b) were acquired for n-fullerene and p-Co_3O_4, respectively. Especially, the photocurrent response of p-n sensitized heterostructure Co_3O_4/fullerene was improved to ca. 5.6 μA (Figure 2D, curve c) that was approximately 6-fold enhancement versus that of fullerene alone. As depicted in Table S3 in the Supporting Information, this sensitization efficiency was higher than the efficiency of yet reported researches for fullerene sensitization. Likewise, as shown in Figure 2E, the transient

photocurrent response for Co_3O_4/fullerene was further investigated, which illustrated desirable stability of the photocurrent response for Co_3O_4/fullerene.

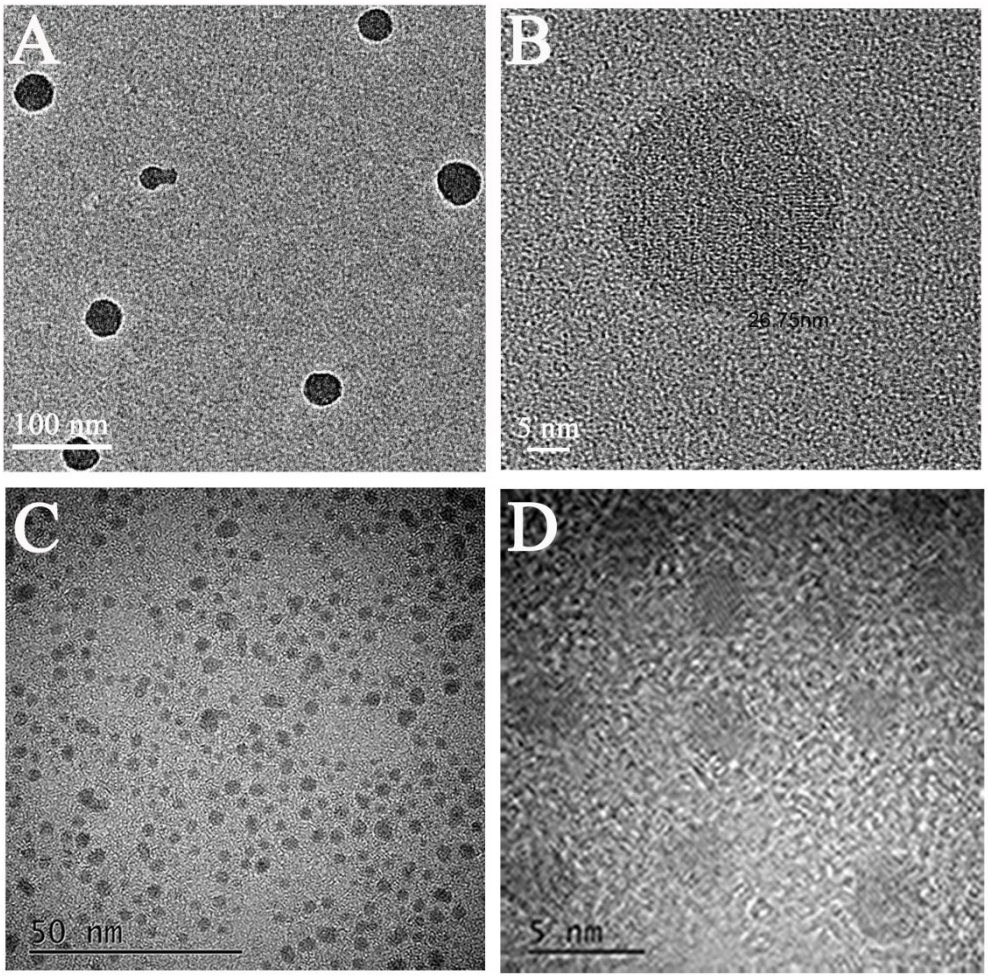

Figure 1. TEM images of (A) fullerene and (C) Co_3O_4. HRTEM images of (B) fullerene and (D) Co_3O_4.

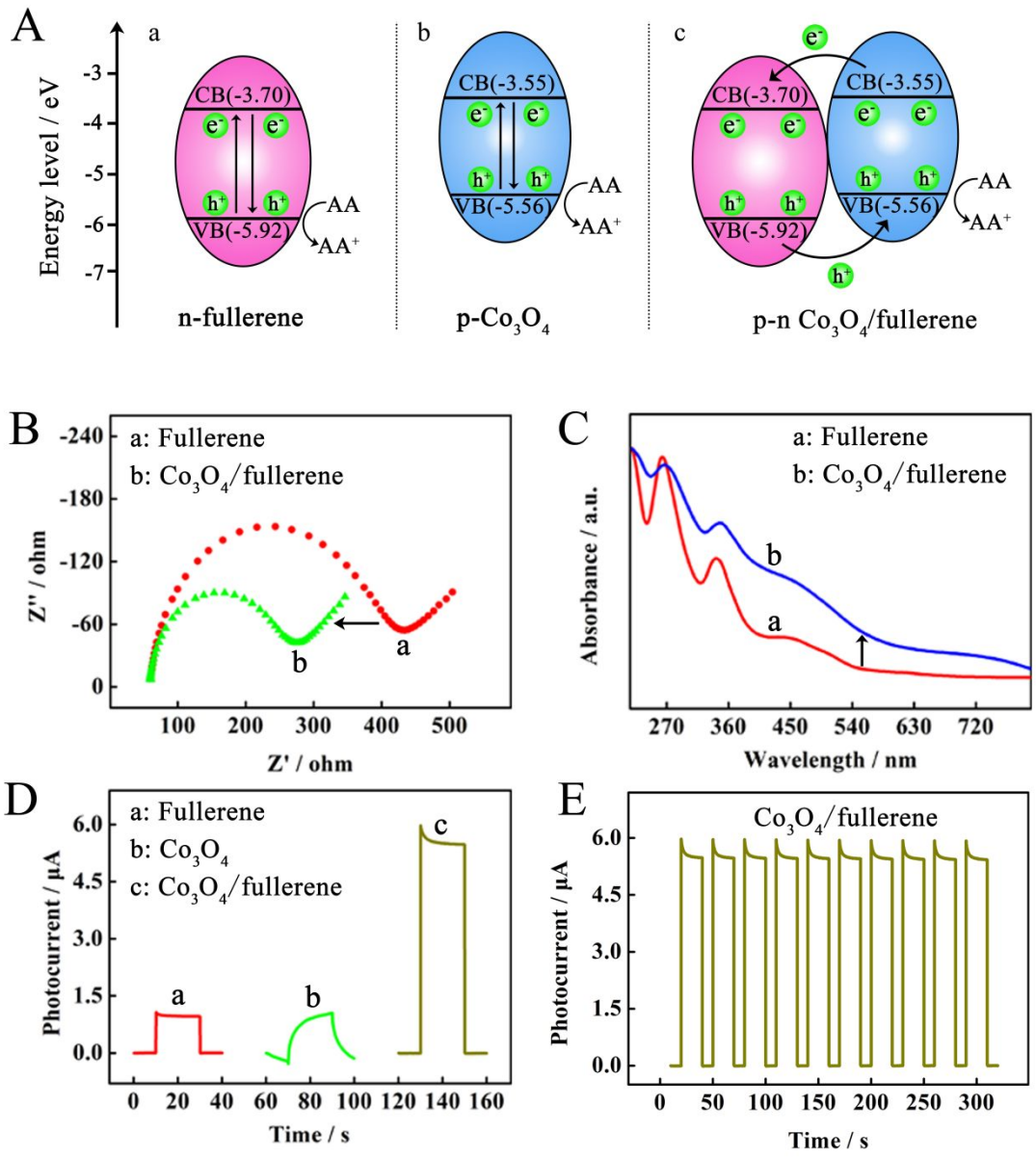

Figure 2. (A) Schematic illustration of the proposed mechanism for the photocurrent responses of (a) n-fullerene, (b) p-Co_3O_4 and (c) p-n Co_3O_4/fullerene; (B) EIS and (C) UV-vis absorption spectrum for (a) fullerene and (b) Co_3O_4/fullerene, respectively; (D) photocurrent intensity for (a) fullerene, (b) Co_3O_4 and (c) Co_3O_4/fullerene; (E) transient photocurrent response for Co_3O_4/fullerene. The EIS were measured in 3 mL PBS (pH 7.0, 0.1 M) including 5.0 mM $[Fe(CN)_6]^{3-/4-}$ and 0.1 M KCl at the frequency from 10^{-2} to 10^6 Hz, an amplitude of 10 mV, and a bias potential of 0.10 V versus saturated calomel electrode under light irradiation of 590 nm wavelength. Fullerene with same final concentrations was employed for the UV-vis measurements in the absence and presence of Co_3O_4. The procedure of transient photocurrent response was

conducted under a light irradiation of periodic "off-on-off" mode for 10 cycles.

Investigation of Optical Band Gap (E_g), Valence Band (VB) and Conduction Band (CB) for the Photoactive Nanomaterials.

The optical methods and electrochemical measurements were performed to determine the energy levels of photoactive nanomaterials, in which ferrocene with an assumed vacuum level of 4.8 eV was usually regarded as the reference substrate.[28] Specifically, the onset absorption wavelength (λ_{onset}) in the ultraviolet-visible (UV-vis) absorption spectrum and oxidation peak in the cyclic voltammetry (CV) curve of the related photoactive nanomaterials were employed to estimate the E_g and the E_{VB}, respectively, according to the empirical formula as follow:

$$E_g = 1240 / \lambda_{onset};$$

$$E_{VB} = -(4.8 + E_{oxidation} - E_{1/2(reference)});$$

$$E_{CB} = E_{VB} + E_g.$$

Based on these, the E_g of n-fullerene and p-Co_3O_4 were estimated to 2.22 eV and 2.01 eV, respectively, as the λ_{onset} were 559 nm for n-fullerene (Figure 3A) and 615 nm for p-Co_3O_4 (Figure 3B). In Figure 3C, the onset oxidation position for the reference agent ferrocene (E_a), n-fullerene (E_b) and p-Co_3O_4 (E_c) showed 0.48 V, 1.60 V and 1.24 V, respectively; thus the E_{VB} of n-fullerene and p-Co_3O_4 were calculated to -5.92 eV and -5.56 eV, respectively, then the E_{CB} of -3.70 eV and -3.55 eV could be determined for n-fullerene and p-Co_3O_4, respectively. All the measurement results and achievements of estimated energy levels were demonstrated in the Table 1.

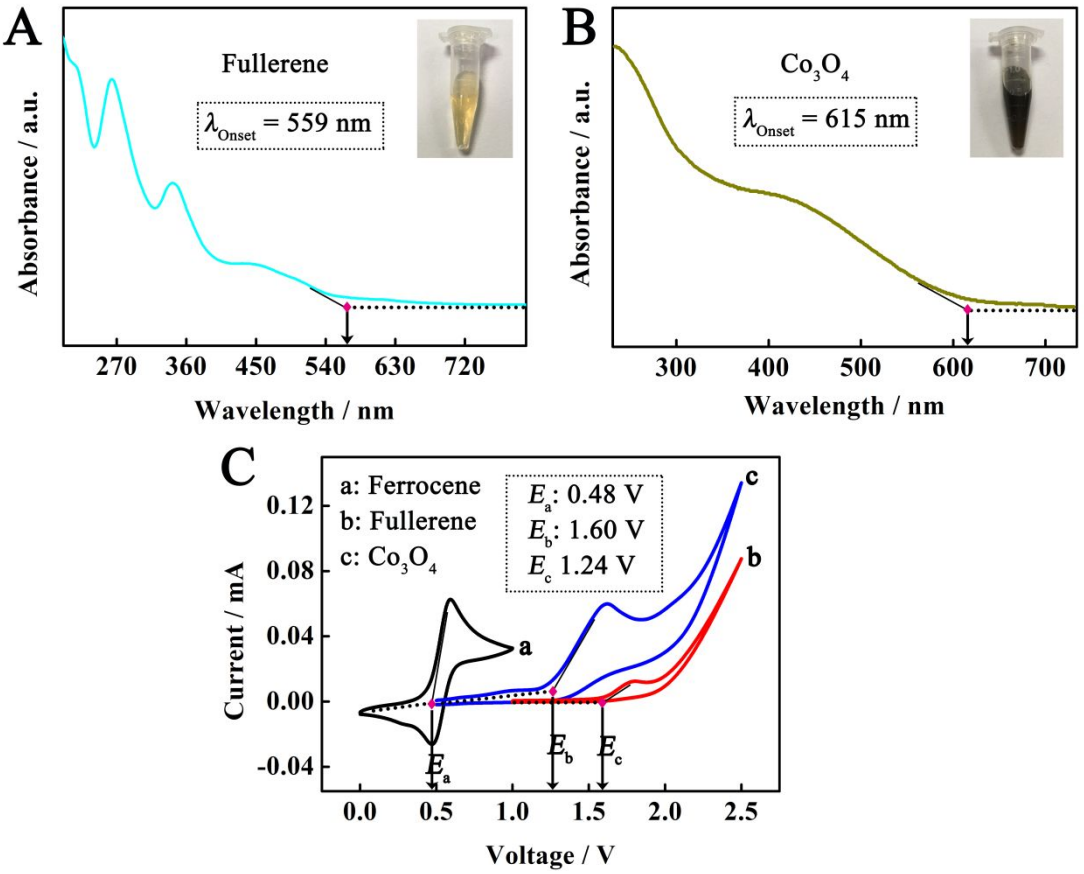

Figure 3. UV-vis absorption spectrum for (A) fullerene and (B) Co_3O_4. Insert showed the original solution of fullerene dispersed in deionized water and Co_3O_4 dispersed in absolute ethanol. (C) CV curves of (a) ferrocene, (b) fullerene and (c) Co_3O_4. The CV measurements were conducted in 4 mL tetrahydrofuran (≥ 99.9%) solution using 0.1 M tetrabutylammonium hexafluorophosphate as a supporting electrolyte at 50 mV/s with referring to Ag/AgCl (with saturated KCl) electrode, in which 0.05 mM ferrocene was used as the horizontal scale.

Table 1. The measurements results and the estimated energy levels for n-fullerene and p-Co_3O_4.

Substrate	λ_{onset}	$E_{1/2(reference)}$	$E_{oxidation}$	E_g	E_{VB}	E_{CB}
n-fullerene	559 nm	0.48 V	1.60 V	2.22 eV	-5.92 eV	-3.70 eV
p-Co_3O_4	615 nm	0.48 V	1.24 V	2.01 eV	-5.56 eV	-3.55 eV

Mechanism of Photocurrent Response for the Different Photoactive Nanomaterials.

In accordance with the estimated E_g, E_{VB} and E_{CB} of fullerene and Co_3O_4, feasible

mechanisms of photocurrent responses of p-fullerene, n-Co_3O_4 and p-n sensitized heterostructure Co_3O_4/fullerene were proposed. In a typical procedure, under 590 nm light irradiation, the photogenerated electron (e^-) could migrate from the VB to the CB of fullerene, and then travel to the surface of GCE. Meanwhile, the photogenerated hole (h^+) in the VB of fullerene could be subsequently captured by ascorbic acid (AA) as the sacrificial agent. Thereby, the electron transmission path was complete, resulting to a photocurrent response (Figure 2A, scheme a). A similar charge separation and transmission processes was raised for Co_3O_4 in scheme b of Figure 2A. Unfortunately, the existence of high e^--h^+ recombination for such single photoactive material seriously restricts the photoelectric conversion efficiency, and thereby sluggish photocurrent intensity could only appeared.[29, 30] Individually, based on the successful construction of p-n sensitized heterostructure Co_3O_4/fullerene, a markedly novel mechanism was been advanced. As scheme c of Figure 2A depicted, interestingly, the e^- in the CB of Co_3O_4 could typically transferred to the CB of fullerene, and then traveled to the surface of GCE. Simultaneously, the h^+ in the VB of fullerene migrated to the VB of Co_3O_4, subsequently captured by AA. The transition of e^- and h^+ contributed to the efficient charge separation of fullerene, resulting in a promising photocurrent response. However, in the presence of SiO_2 NPs, a violent increment of steric hindrance on the surface of the modified electrode strongly blocked the electron transmission from AA to the p-n sensitized heterostructure Co_3O_4/fullerene, causing an interruption of the electron transmission path. Thus, the initial photocurrent intensity was sharply decreased.

CV and PEC Characterizations of the PEC Biosensor.

The construction process of the PEC biosensor was characterized by CV measurements,

which was illustrated in Figure 4A. The bare GCE showed a pair of ideal redox peak (curve a), and then the peak current (curve b) decreased after the modification of fullerene owning to the effect of fullerene to hinder electron transmission. When the Co_3O_4 was incubated, an apparent increment of the peak current (curve c) was gotten, which was attributed that the p-n heterostructure Co_3O_4/fullerene could accelerate electron transmission, in accordance with the admirable conductivity shown in the EIS characterization in Figure 2A. Subsequently, dep Au was conducted, and the peak current increased (curve d) owing to the excellent conductivity of Au. With the anchor of the mixture of SD-SiO_2/DW-PD, significant decrease of the peak current was obtained (curve e) for a sharp increment of the steric hindrance on the electrode surface. When HT was immobilized on the modified electrode, a consecutive moderate decrement of the peak current (curve f) was obtained due to the steric effect of the small molecular. At last, after the incubation of Nb.BbvCI/output DNA, the redox peak current (curve g) demonstrated an obvious increment, which was attributed that the conductive properties of the modified electrode surface restored effectively after the valid cancellation of the steric hindrance.

Further conformation about the construction for the PEC biosensor were obtained with the photocurrent responses. Figure 4B showed that the photocurrent response of the bare GCE was near to zero (curve a), while the coat of fullerene onto the electrode led to a sluggish photocurrent response (curve b) as a result of the restricted charge separation of fullerene. Then the immobilization of Co_3O_4 caused a distinguished enhancement of the photocurrent response (curve c) for the illustriously sensitized effect of Co_3O_4 towards fullerene. Next, after the step of dep Au, a further increment of the photocurrent response was found (curve d) thanks to the

excellent conductivity of Au and plasmonic effect in the obtained modified electrode (corresponding mechanism was available in Figure S7 in the Supporting Information).[31] Yet, the mixture of SD-SiO_2/DW-PD was anchored, and the photocurrent response (curve e) expressed an incisive decrement because the enriched quencher elements SiO_2 introduced a sharp appearance of steric hindrance on the modified electrode surface, causing the powerful depression against the electron transmission. Afterwards, as HT was attached to the modified electrode, the photocurrent response (curve f) was drawn in a slight decrement due to the introduction of steric hindrance effect. Finally, it was noticeable that the incubation of Nb.BbvCI/output DNA brought about a distinct recovery towards the photocurrent response (curve g), attributing to the reality that the great lay-off of SiO_2 considerably reduced the steric hindrance on the modified electrode surface. These results suggested the PEC biosensor was fabricated successfully.

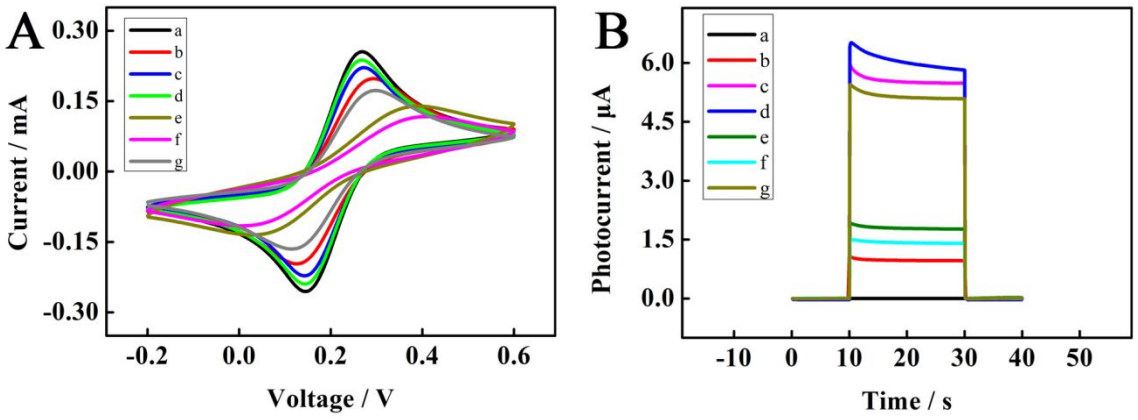

Figure 4. (A) CV characterizations and (B) PEC characterizations of (a) bare GCE, (b) fullerene/GCE, (c) Co_3O_4/fullerene/GCE, (d) dep Au/Co_3O_4/fullerene/GCE, (e) DW-PD/SD-SiO_2/dep Au/Co_3O_4/fullerene/GCE, (f) HT/DW-PD/SD-SiO_2/dep Au/Co_3O_4/fullerene/GCE, (g) Nb.BbvCI/output DNA/HT/DW-PD/SD-SiO_2/dep Au/Co_3O_4/fullerene/GCE. The PEC procedure was conducted under the excitation of a light-emitting diode lamp with the wavelength of 590 nm and switch mode "off-on-off" of 10

s-20 s-10 s at 0.2 V potential in 4 mL PBS (pH 7.0, 0.1 M) containing 1 M freshly prepared AA as the sacrifice reagent. The CV measurements were implanted in 3 mL PBS (pH 7.0, 0.1 M) containing 5.0 mM $[Fe(CN)_6]^{3-/4-}$ and 0.1 M KCl between -0.2 and 0.6 V at a scan rate of 50 mV/s. The saturated calomel electrode was used as the horizontal scale reference.

Detection Analysis of the PEC Biosensor.

Target DNA with a series of different concentrations were employed for evaluating the analytical function of the proposed PEC biosensor. As expected, a gradual enhancement of the photocurrent response was ascribed along with the increment of the target concentration with this system. Figure 5A and Figure 5B depicted that the linear equation was corrected to $I = -0.5208 \lg c + 5.628$ (where the elements of I and c were the photocurrent intensity and the target concentration, respectively) with a correlation coefficient (R^2) of 0.9962, and the liner range showed from 60 aM to 1×10^5 aM with a detection limit of 20 aM (defined as the signal-to-noise of 3). Furthermore, after an observant comparison study for the detection property of our PEC biosensor with yet published literatures towards oligonucleotides estimation in Table S4 in the Supporting Information, our proposed PEC biosensor indicated a pretty wider liner range as well as a lower detection limit, which was mainly attributed to the versatile construction of the target-cascade signal amplification strategy and the p-n sensitized heterostructure platform.

To survey the selectivity of the proposed PEC biosensor, target DNA (1 pM) with its interferences containing smDNA 1 (100 pM), smDNA 2 (100 pM), dmDNA (100 pM) and the mixture sequences were used as models. As illustrated in Figure 5C, the introduction of target DNA and the mixture sequences led to an apparent quench towards the photocurrent response,

while no obvious change of the photocurrent response was given after adding smDNA 1, smDNA 2 and dmDNA, demonstrating that the proposed PEC biosensor possessed excellent selectivity. The stability of the PEC biosensor was completed under a light irradiation of periodic "off-on-off" mode for 10 cycles with 1 pM target DNA. Figure 5D showed that the obtained photocurrent intensity with the relative standard deviation (RSD) of 2.16% exhibited high consistency and stability, which indicated that the presented PEC biosensor owned exceptional stability.

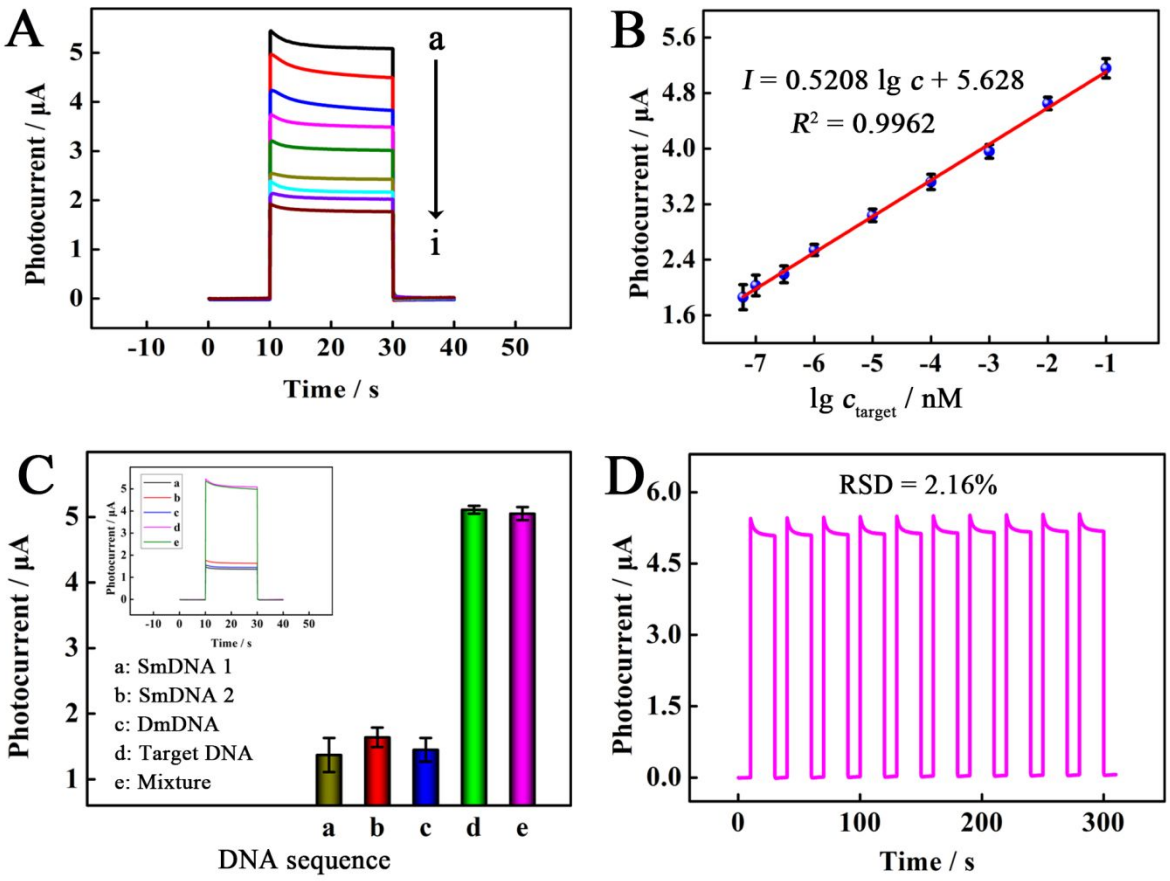

Figure 5. (A) Photocurrent responses of the PEC biosensor towards target at different concentrations (from top to bottom): (a) 100 pM, (b) 10 pM, (c) 1 pM, (d) 100 fM, (e) 10 fM, (f) 1 fM, (g) 0.3 fM, (h) 0.1 fM and (i) 0.06 fM; (B) linear relationship between photocurrent responses and the logarithm of the target concentration; (C) selectivity with photocurrent responses in insert for incubating different samples and (D)

stability of the PEC biosensor.

Conclusion

In summary, an ultrasensitive PEC biosensor was described based on the p-n sensitized heterostructure Co_3O_4/fullerene photoactive material and its quencher element SiO_2 as the photocurrent indicator accompanying the target-cascade signal amplification strategy, which was successfully adopted for the quantitative investigation of the target DNA (a fragment of p53 gene) and exhibited promising detection performance. Loading discrete p-Co_3O_4 as efficient sensitizer on n-fullerene C_{60} surface as photoactive substrate *via* layer-by-layer attachment, a novel p-n sensitized heterostructure Co_3O_4/fullerene with high PEC performance and improved photoelectric conversion efficiency was established. Notably, despite both n-fullerene and p-Co_3O_4 respectively exhibited clumsy photocurrent responses by themselves, a stable photocurrent intensity of 6-fold enhancement versus fullerene alone was founded for the constructed p-n sensitized heterostructure Co_3O_4/fullerene, which achieved the highest level among the intensely sensitization researches towards fullerene, making it an interesting candidate for advanced PEC biosensing. Through the combination employment of the nicking endonuclease signal amplification and the 3-D DNA Walker recycle amplification, the well-designed target-cascade signal amplification strategy brought about extremely effective signal amplification of the target, making senses for the reduced detection limit and the expanded linear range. These were enjoyably in accordance with the outstanding detection results in this work, showing the detection liner range from 60 aM to 1×10^5 aM and a detection limit of 20 aM. We believed the fabricated PEC biosensor put forward a universal conception in the construction of novel sensitized heterostructure, and could be developed as a useful instrument

for ascendant application in biomolecular examinations.

Supporting Information

Materials and reagents, Apparatus, Synthesis of Fe_3O_4@Au Nanoparticles (NPs) and SiO_2-NH_2, Optimization of Experimental Conditions for the PEC Measurement, Experimental Conditions, Characterizations of the SiO_2 and Bioconjugates, PAGE Characterization for 3-D DNA Walker Amplification, Preliminary Application of the PEC Biosensor, Other Tables and Figures.

Notes

The authors declare no competing financial interest.

Acknowledge

This work was financially supported by the National Natural Science Foundation of China (21775124, 21575116 and 21675129) and the Fundamental Research Funds for the Central Universities (XDJK2018AA003), China.

References

1. Li, M. J.; Liang, W. B.; Yuan, R.; Chai, Y. Q. CdTe QD-CeO_2 Complex as a Strong Photoelectrochemical Signal Indicator for the Ultrasensitive microRNA Assay. *ACS Appl. Mater. Interfaces* **2019**, *11*, 11834-11840.

2. Zhen, R. J.; Luo, Z. B.; Su, L. S.; Zhang, L. J.; Tang, D. P.; Niessener, R.; Knopp, D. Palindromic Molecular Beacon Based Z-Scheme BiOCl-Au-CdS Photoelectrochemical Biodetection. *Anal. Chem.* **2019**, *91*, 2447-2454.

3. Wang, D. D.; Chen, L. P.; Liu. J.; Guan, F. Y.; Sun, R. Z.; Jiang, L.; Feng, X. J. A Reliable Photoelectrochemical Bioassay System Based on Cathodic Reaction at a Solid-Liquid-Air Joint

Interface. *Adv*. *Funct*. *Mater*. **2018**, *28*, 1804410.

4. Ibrahim, I.; Lim, H. N.; Huang, N. M.; Pandikumar, A. Cadmium Sulphide-Reduced Graphene Oxide-Modified Photoelectrode-Based Photoelectrochemical Sensing Platform for Copper(II) Ions. *PLoS One* **2016**, *11*, e0154557.

5. Shu, J.; Tang, D. P. Current Advances in Quantum-Dots-Based Photoelectrochemical Immunoassays. *Chem. Asian J.* **2017**, *12*, 2780-2789.

6. Foo, C. Y.; Lim, H. N.; Pandikumar, A.; Huang, N. M.; Ng, Y. H. Utilization of reduced graphene oxide/cadmium sulfide-modified carbon cloth for visible-light-prompt photoelectrochemical sensor for copper (II) ions. *Journal of Hazardous Materials* **2016**, *304*, 400-408.

7. Lv, S. Z.; Zhang, K. Y.; Zeng, Y. Y.; Tang, D. P. Double Photosystems-Based 'Z-Scheme' Photoelectrochemical Sensing Mode for Ultrasensitive Detection of Disease Biomarker Accompanying Three-Dimensional DNA Walker. *Anal. Chem.* **2018**, *90*, 7086-7093.

8. Luo, Z. B.; Qi, Q. G.; Zhang, L. J.; Zeng, R. J.; Su, L. S.; Tang, D. P. Branched Polyethylenimine-Modified Upconversion Nanohybrid-Mediated Photoelectrochemical Immunoassay with Synergistic Effect of Dual-Purpose Copper Ions. *Anal. Chem.* **2019**, *91*, 4149-4156.

9. Qiu, Z. L.; Shu, J.; Liu, J. F.; Tang, D. P. Dual-Channel Photoelectrochemical Ratiometric Aptasensor with up-Converting Nanocrystals Using Spatial-Resolved Technique on Homemade 3D Printed Device. *Anal. Chem.* **2019**, *91*, 1260-1268.

10. Zhang, Y. F.; Xu, R.; Kang, Q.; Zhang, Y.; Wei, Q.; Wang, Y. G.; Ju, H. X. Ultrasensitive Photoelectrochemical Biosensing Platform for Detecting N-Terminal Pro-brain Natriuretic

Peptide Based on SnO_2/SnS_2/mpg-C_3N_4 Amplified by PbS/SiO_2. *ACS Appl. Mater. Interfaces* **2018**, *10*, 31080-31087.

11. Wu, R.; Fan, G. C.; Jiang, L. P.; Zhu, J. J. Peptide-based Photoelectrochemical Cytosensor Using a Hollow TiO_2/EG/$ZnIn_2S_4$ Cosensitized Structure for Ultrasensitive Detection of Early Apoptotic Cells and Drug Evaluation. *ACS Appl*. *Mater*. *Interfaces* **2018**, *10*, 4429-4438.

12. Liu, Y.; Yan, K.; Zhang, J. D. Graphitic Carbon Nitride Sensitized with CdS Quantum Dots for Visible-Light-Driven Photoelectrochemical Aptasensing of Tetracycline. *ACS Appl*. *Mater*. *Interfaces* **2016**, *8*, 28255-28264.

13. Li, R. Y.; Zhang, Y.; Tu, W. W.; Dai, Z. H. Photoelectrochemical Bioanalysis platform for Cells Monitoring Based on Dual Signal Amplification Using in Situ Generation of Electron Acceptor Coupled with Heterojunction. *ACS Appl*. *Mater*. *Interfaces* **2017**, *9*, 22289-22297.

14. Wang, H. H.; Li, M. J.; Zheng, Y. N.; Hu, T.; Chai, Y. Q.; Yuan, R. An Ultrasensitive Photoelectrochemical Biosensor Based on $[Ru(dcbpy)_2dppz]^{2+}$/Rose Bengal Dyes Co-Sensitized Fullerene for DNA Detection. *Biosens*. *Bioelectron*. **2018**, *120*, 71-76.

15. Fan, G. C.; Zhao, M.; Zhu, H.; Shi, J. Jun.; Zhang, J. R.; Zhu, J. J. Signal-On Photoelectrochemical Aptasensor for Adenosine Triphosphate Detection Based on Sensitization Effect of CdS:Mn@$Ru(bpy)_2$(dcbpy) Nanocomposites. *J. Phys*. *Chem*. *C* **2016**, *120*, 15657-15665.

16. Tu, W. W.; Cao, H.; Zhang, L.; Bao, J.; Liu, X.; Dai, Z. H. Dual Signal Amplification Using Gold Nanoparticles-Enhanced Zinc Selenide Nanoflakes and p19 Protein for Ultrasensitive Photoelectrochemical Biosensing of MicroRNA in Cell. *Anal*. *Chem*. **2016**, *88*, 10459-10465.

17. Burlingame, Q.; Coburn, C.; Che, X.; Panda, A.; Qu, Y.; Forrest, S. R. Centimetre-Scale Electron Diffusion in Photoactive Organic Heterostructures. *Nature* **2018**, *554*, 77-80.

18. Yu, X.; Marks, T.; Facchetti, A. Metal Oxides for Optoelectronic Applications. *Nature Mater*. **2016**, *15*, 383-396.

19. Kupfer, B.; Majhi, K.; Keller, D. A.; Bouhadana, Y.; Ruhle, S.; Barad, H. N.; Anderson, A. Y.; Zaban, A. Thin Film Co_3O_4/TiO_2 Heterojunction Solar Cells. *Adv*. *Energy Mater*. **2014**, *5*, 1401007.

20. Yang, J.; Cooper, J. K.; Toma, F. M.; Walczak, K. A.; Favaro, M.; Beeman, J. W.; Hess, L. H.; Wang, C.; Zhu, C.; Gul, S.; Yano, J.; Kisielowski, C.; Schwartzberg, A.; Sharp, I. D. A Multifunctional Biphasic Water Splitting Catalyst Tailored for Integration with High-Performance Semiconductor Photoanodes. *Nature Mater*. **2017**, *16*, 335-341.

21. Chang, X. X.; Wang, T; Zhang, P.; Zhang, J. J.; Li, A.; Gong, J. L. Enhanced Surface Reaction Kinetics and Charge Separation of p-n Heterojunction $Co_3O_4/BiVO_4$ Photoanodes. *J. Am*. *Chem*. Soc. **2015**, *137*, 8356-8359.

22. Han, H. S.; Shin, S.; Kim, D. H.; Park, I. J.; Kim, J. S.; Huang, P. S.; Lee, J. K.; Cho, I. S.; Zheng, X. L. Boosting the Solar Water Oxidation Performance of a $BiVO_4$ Photoanode by Crystallographic Orientation Control. *Energy Environ. Sci.* **2018**, *11*, 1299-1306.

23. Yang, Z. Q.; Wang, Y.; Zhang, D.; Chen, C. A Sensitizing Photoelectrochemical Sensing Platform Strategy Based on Bioetching Preparation of Bi_2S_3/BiOCl p-n Heterojunction. *Talanta* **2018,** *190*, 357-362.

24. Shao, Y. C.; Xiao, Z. G.; Bi, C.; Yuan, Y. B.; Huang, J. S. Origin and Elimination of Photocurrent Hysteresis by Fullerene Passivation in $CH_3NH_3PbI_3$ Planar Heterojunction Solar

Cells. *Nat. Commun.* **2014**, 5, 5784.

25. Kim, K.; Lee, T. H.; Santos, E. J. G.; Jo, P. S.; Salleo, A.; Nishi, Y.; Bao, Z. Structural and Electrical Investigation of C_{60}-Graphene Vertical Heterostructures. *ACS Nano* **2015**, *9*, 5922-5928.

26. Ge, L.; Wang, W. X.; Hou, T.; Li, F. A Versatile Immobilization-Free Photoelectrochemical Biosensor for Ultrasensitive Detection of Cancer Biomarker Based on Enzyme-Free Cascaded Quadratic Amplification Strategy. *Biosens. Bioelectron.* **2016**, *77*, 220-226.

27. Saha, S.; Chan, Y.; Soleymani, L. Enhancing the Photoelectrochemical Response of DNA Biosensors Using Wrinkled Interfaces. *ACS Appl. Mater. Interfaces* **2018**, *10*, 31178-31185.

28. Wang, Q.; Ruan, Y. F.; Zhao, W. W.; Lin, P.; Xu, J. J.; Chen, H. Y. Semiconducting Organic-Inorganic Nanodots Heterojunctions: Platforms for General Photoelectrochemical Bioanalysis Application. *Anal. Chem*. **2018**, *90*, 3759-3765.

29. Kongkanand, A.; Tvrdy, K.; Takechi, K.; Kuno, M.; Kamat, P. V. J. Quantum Dot Solar Cells. Tuning Photoresponse through Size and Shape Control of CdSe-TiO_2 Architecture. *J. Am. Chem. Soc.* **2008**, *130*, 4007-4015.

30. Zhang, P.; Guan, B. Y.; Yu, L.; Lou, X. W. Facile Synthesis of Multi-shelled ZnS-CdS Cages with Enhanced Photoelectrochemical Performance for Solar Energy Conversion. *Chem* **2018**, *4*, 162-173.

31. Ibrahim, I.; Lim, H. N.; Abou-Zied, O. K.; Huang, N. M.; Estrela, P.; Pandikumar, A. Cadmium Sulfide Nanoparticles Decorated with Au Quantum Dots as Ultrasensitive Photoelectrochemical Sensor for Selective Detection of Copper(II) Ions. *J. Phys. Chem. C* **2016**,

120, 22202-22214

For TOC Only:

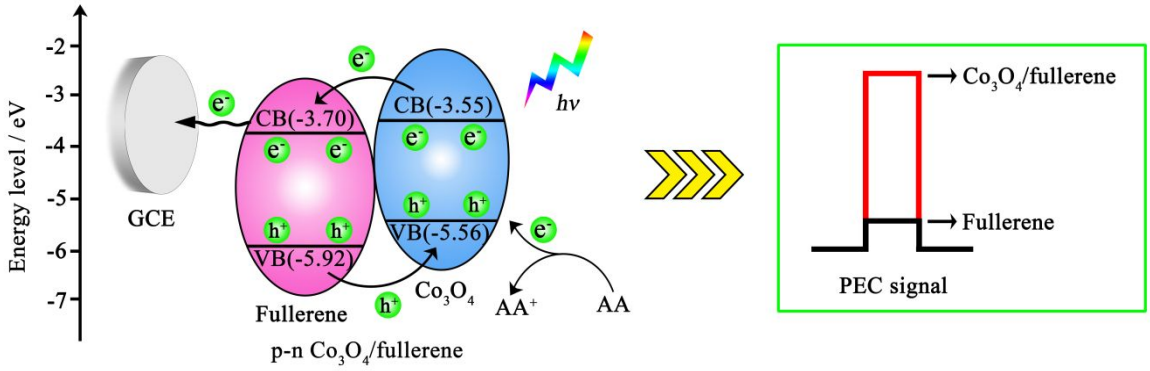
Energy level / eV
-2
-3
-4
-5
-6
-7
GCE
CB(-3.70)
VB(-5.92)
Fullerene
CB(-3.55)
VB(-5.56)
Co3O4
hv
AA+
AA
p-n Co3O4/fullerene
Co3O4/fullerene
Fullerene
PEC signal